Green Chemistry

Accepted Manuscript

ROYAL SOCIETY OF CHEMISTRY

www.rsc.org/greenchem

Journal Name

ARTICLE

7.1% efficienct co–electroplated Cu_2ZnSnS_4 thin film solar cells with sputtered CdS buffer layers

Received 00th January 20xx,
Accepted 00th January 20xx

DOI: 10.1039/x0xx00000x

www.rsc.org/

Jiahua Tao,[a] Junfeng Liu,[a] Leilei Chen,[a] Huiyi Cao,[a] Xiankuan Meng,[a] Yingbin Zhang,[a] Chuanjun Zhang,[b] Lin Sun,[a] Pingxiong Yang[a] and Junhao Chu[ab*]

Cu_2ZnSnS_4 (CZTS) thin films with fine control over composition and pure phase were fabricated by sulfurization of co–electroplated Cu–Zn–Sn–S precursors. We have systematically investigated the concentration of Cu(II) ion can influence the properties of CZTS absorber layers and the photovoltaic performance of resulting solar cell devices. The results indicate that increasing Cu(II) concentration almost linearly increases the Cu content in the final CZTS thin films, greatly enhances the (112) preferred orientation, significantly improves the crystallinity of the absorber layer, remarkably reduces the ZnS secondary phase, and hence improves their photovoltaic performance. However, upon further increase the Cu(II) concentration degrades the crystal quality of the absorber layer, and forms the CuS_x secondary phase, which is quite detrimental to device photovoltaic performance. Here we introduce a novel sputtered CdS buffer layer for the CZTS solar cells. For the first time, co–electrodeposited CZTS solar cells exceed the 7% efficiency threshold. These findings offer new research directions for solving persistent challenges of chemical bath deposition of CdS in CZTS solar cells.

1. Introduction

Kesterite copper zinc tin chalcogenide Cu_2ZnSnS_4 (CZTS) has recently attracted intensive attention as an important photovoltaic material for scalable production of thin–film solar cells due to its earth–abundant and non–toxic elements, and an optimal direct band gap with the predicted theoretical maximum efficiency of 32.4% (J_{sc}=29.6 mA cm^{-2}, V_{oc}=1.21 V, FF=89.9% and E_g=1.48 eV).[1–4] To date, the reported highest power conversion efficiencies (PCEs) for the pure sulfide CZTS, pure selenide $Cu_2ZnSnSe_4$ (CZTSe) and mixed sulfo-selenide $Cu_2ZnSn(S,Se)_4$ (CZTSSe) have reached 8.5%,[5] 11.6%,[6] and 12.6%,[5,7] respectively, which however is lower than that of $Cu(In,Ga)Se_2$ (21.7%) and CdTe (21.0%) solar cells.[5] To improve the PCE of CZTSSe solar cells, they are usually prepared by adjustment the ratio of Se/S to obtain the tunable band gap from 1.0 to 1.5 eV during a harmful selenization process.[2,8-15] Chen et al. calculated that the high-efficiency CZTSSe solar cells based on absorber layers with high Se content reduce the bandgap and thus CZTSSe solar cells with high Se content have better photogenerated current than CZTS solar cells (high S content).[16] Fangyang et al. demonstrated a PCE of CZTS solar cells can be improved from 5.73% to 8.25% through optimizing the ratio of S/(S+Se).[17] Recently Zhenghua et al. reported the fabrication of CZTS solar cells with a PCE of 9.24% using doping Cd into CZTS thin films to form $Cu_2Zn_{1-x}Cd_xSnS_4$ (CZCTS) thin films with tunable direct band gaps.[18] Although the PCE of CZTS solar cells is much less that of CZTSe, CZTSSe and CZCTS solar cells, the continued development of more environment friendly and large-scale photovoltaic processes for CZTS solar cells is essential because they do not use toxic Se and Cd elements.

Various deposition methods have being developed for the fabrication of CZTS absorber layer, both vacuum–based and non–vacuum solution–based deposition approaches, have yielded a range of efficiency levels. However, the control of the pure-phased CZTS absorber layer with a Cu–poor and Zn–rich condition is an extremely challenging task, largely due to the narrow compositional stability window of the kesterite compound.[19] Thus making the precise control and adjustment of the composition, phase, and properties of the absorber material is very important in producing high–efficiency CZTS solar cells. The vacuum–based deposition approach for the preparation of CZTS solar cells is currently based on sputtering of the suitable metal precursor layers or on co–evaporation of the individual metallic elements followed by sulfurization at high temperature in the presence of S vapor and/or H_2S gas. Specifically, Katagiri et al. reported a PCE of 6.77% for CZTS solar cells with the element ratio of Cu/(Zn+Sn)=0.85 and Zn/Sn=1.25 prepared by co–sputtering metallic precursors followed by sulfurizing in H_2S.[20] So far, Shin et al. reported a record PCE of 8.4% using a ultra–thin CZTS absorber having the element ratio of Cu/(Zn+Sn)=0.78 and Zn/Sn=1.25 via a thermal co–evaporation method.[21] The advantage of these high-vacuum deposition techniques is the versatility afforded by the integration of multiple evaporation or sputtering sources, thereby leading to good control over the film composition

[a] Key Laboratory of Polar Materials and Devices, Ministry of Education, Department of Electronic Engineering, East China Normal University, Shanghai 200241, China. E-mail address: jhchu@mail.sitp.ac.cn (JH. Chu)
[b] National Laboratory for Infrared Physics, Shanghai Institute of Technical Physics, Chinese Academy of Sciences, Shanghai 200083, China
† Footnotes relating to the title and/or authors should appear here.
Electronic Supplementary Information (ESI) available: Experimental, composition analysis, XRD and Raman spectra (325 nm excitation), High-resolution XPS analysis, additional J–V characteristics and optical transmittance spectra. See DOI: 10.1039/x0xx00000x

and phase profile. However, vacuum conditions necessitate an evacuated confined space, which is not conducive to the cost-effective deposition of uniform films over large-area substrates. Furthermore, these techniques generally suffer from relatively slow throughput, low materials utilization and considerable energy expenditure to heat or sputter from the target sources. For these critical issues, alternatively, several non–vacuum approaches, such as hydrazine–based approach,[7,9–12,15] sol–gel method[8,17,18,22-25] and electrodeposition[26–31] could offer a low–cost route for preparing CZTS absorber layers.

Among these techniques, the electrodeposition approach has received a great deal of attention in recent years because of its simplicity, low equipment cost, cheap raw materials and room temperature growth. Furthermore, there is no need to use toxic solvents or ligands like hydrazine. Generally this approach can be further divided into two groups: (i) stacked elemental layer,[26,27] and (ii) co–electrodeposited layer.[28-31] For instance, an outstanding PCE of 7.3% has been achieved using stacked electroplated CZTS absorber layers with Cu/Sn=1.83, Cu/(Zn+Sn)=0.78 and Zn/Sn=1.35.[26] Recently, a high PCE of 7.99% (active area: 0.03 cm^{-2}) has been reached for the stacked electrodeposition CZTS solar cells with Cu–poor and Zn–rich (Cu content=0.23, Zn/Sn=1.2) that were fabricated from preheated Cu/Zn/Sn metallic stack precursors.[27] This metal stack approach manifests the precise control of compositional uniformity through the accurate manipulation of the thickness of metal layers on the nanoscale. Current issue for metal stacked precursor is the morphology of Sn precursor is very rough compared to the other elemental precursors. In addition, the poor morphology of CZTS is due to non-uniform nucleation of Zn precursor. We have recently reported that CZTS solar cells can be co–electrodeposited CZTS absorber layers with Cu/(Zn+Sn)=0.82 and Zn/Sn=1.31, the best yielding 6.6% efficiency.[28] Compared to the stacked elemental approach, co-electrodeposition approach has not been thoroughly investigated even though the simply fabrication process of the precursor is one of its significant advantages.

Based on these above-mentioned results indicate that CZTS absorber layers having Cu–poor and Zn–rich makeup result in high–efficiency solar cells. One of the issues in the synthesis of CZTS compound is there exists a narrow kesterite phase stability region,[19] and the exquisite controllability over composition and phase is critical in achieving high quality CZTS thin films. Influence of the Cu content on the grain growth is quite controversial: an improvement of the crystallinity of co-evaporated CZTS thin films with the increase of the copper content has been observed,[32] whereas the opposite trend is seen for the sol–gel processed CZTS thin films.[25] As far as we know, very few investigations on the metal salt concentration (e.g., Cu (II), Zn (II) and Sn (II) ions) in the co–electroplated CZTS precursors have been reported, so we have systematically investigated the influence of Cu (II) ion on the formation process of CZTS thin films and devices performance. Interestingly, it is found that the increase in Cu (II) ion results in a notable improvement in the micron-sized grain of final CZTS thin films, in accordance with the same trend also obtained in co-evaporated CZTS thin films,[32] and consequently improves the device efficiency.

To date, high–efficiency CZTS solar cells have been reported where a high–resistivity CdS thin film deposited by the traditional chemical bath deposition (CBD) is always employed as a buffer layer.[6-13,17,18] However, the major drawback is that CBD–CdS buffer layer typically produces the large amount of toxic Cd containing waste. In addition, ammonium hydroxide is usually utilized during the deposition process, which is highly volatile and toxic to human health. Besides, the volatility of ammonia changes the pH of deposition bath solution influenced the performance of the CdS buffer layer. Moreover, a redundant treatment in a wastewater process greatly increases the cost. Therefore, here we report a novel sputtering approach to process CdS buffer layer, which is suitable for reducing the environmental impact and enhancing the continuity of the deposition processes. In this paper, we have demonstrated the successful use of a sputtered CdS buffer layer for CZTS solar cells with high efficiencies as high as those fabricated using CBD–CdS.[21,26-28] To the best of our knowledge, the PCE of 7.1% is the highest value reported to date for CZTS solar cells prepared by co–electrodeposition approach. Moreover, our results offer the possibility to realize environmentally benign, scalable, low-cost and high-efficiency solar cells.

2. Experimental

CZTS thin films were prepared on molybdenum coated glass substrates (3.0×2.5 cm^2, 0.7 μm Mo/glass) by sulfurization of co–electrodeposited Cu–Zn–Sn–S precursors, as detailed in our previous work,[28] with slight changes in the concentrations of the Cu(II) ions. All raw chemicals are of analytical reagent grade (supplied by Sinopharm Chemical Reagent Co. Ltd., China). The precursor solutions were made by simultaneously dissolving metal sulfates of Cu(II) (5–20 mM), Zn(II) (20 mM) Sn(II) (20 mM), tartaric acid (20 mM), trisodium citrate (100 mM) and sodium thiosulfate (10 mM) in non-toxic aqueous solutions (200 mL) at room temperature. The concentration of Cu(II) ion was systematically varied from 5 to 20 mM at an interval of 5 mM. Cyclic voltammetry tests were measured and amperometric I–t curves were recorded at room temperature without stirring using a CHI660D electrochemical workstation (CH Instrument, USA). The Cu–Zn–Sn–S precursors were co–electrodeposited at –1.15 V (vs. Ag/AgCl) for 30 min at room temperature under an air atmosphere. After the deposition, the precursors were then sealed in a rapid thermal process (RTP) furnace containing 0.5 g of sulfur powder with a purity of 99%. The RTP process was heated up to 570 °C (ramp to 570 °C at 5 °C s^{-1}) for 15 min. The sulfurized CZTS thin films were denoted CZTS(05), CZTS(10), CZTS(15) and CZTS(20) corresponding to the Cu(II) concentration.

The sulfurized CZTS absorber layers were employed for the fabrication of complete thin film solar cell devices with a conventional structure of glass/Mo/CZTS/sputtered CdS/i–ZnO/AZO (without an antireflection layer). Notably, prior to CdS deposition, all CZTS thin films were sputtered for 10 min to etch the superficial ZnS secondary phase. A CdS (~150 nm, see Figure S2), i–ZnO (~50 nm) and ZnO: Al (~700 nm) were subsequently deposited by RF magnetron sputtering. Finally, the samples were mechanically scribed into individual cells with a total area of 0.20

cm^2. The structural properties of the prepared CZTS thin films were studied by X–ray diffraction (XRD) using a Bruker D8 Discover diffractometer with Cu K*a* radiation (λ=1.5406 Å). Raman measurements were performed using the 532 nm line of an Ar^+ laser with 50 mW, and the 325 nm line of a He–Cd laser with 0.5 mW as excitation source. The morphologies and chemical compositions were observed using a PhilipsS360 scanning electron microscope (SEM) attached to an energy–dispersive X–ray spectroscope (EDS, accelerating voltage of 20 kV, measured area of 20×20 μm^2). The element components were obtained as the average values between two regions at the surface of the films. X–ray photoelectron spectroscopy (XPS) measurements were performed on a PHI 5000C ESCA system with Mg Kα source at 14.0 kV and 25 mA. All the binding energies were referenced to the contaminant C 1s peak at 284.6 eV of the surface adventitious carbon. The current density–voltage (J–V) characteristics of CZTS solar cells were performed using a continuous light solar cell performance tester system in the dark at 25 °C and under simulated air mass AM1.5 G (100 mW cm^{-2}) using a solar simulator (Xe lamp, Newport). External quantum efficiency (EQE) measurements were performed by a single source illumination system (Qtest Station 1000AD EQE) combined with a monochromator. A calibrated Si–cell was used as reference for the J–V as well as for the EQE measurements.

3. Results and discussion

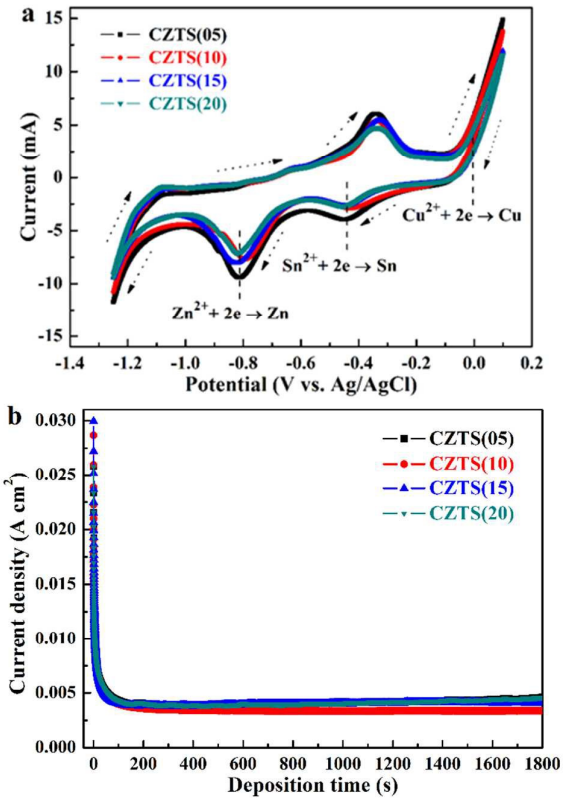

Fig. 1(a) Cyclic voltammetry diagrams of aqueous electrolyte solutions with different Cu(II) concentrations used for co-electroplated Cu–Zn–Sn–S precursors on Mo/glass electrodes, scanned from 0.2 to –1.3 V at a scan rate of 10 mV s^{-1}. Arrows indicate scan directions. (b) The corresponding chronoamperograms during co–electrodeposition with constant potential at –1.15 V (vs. Ag/AgCl) for 30 min.

As copper, zinc and tin elements have the large difference in the standard reduction potentials and reduction kinetics,[31] it is proven to be a challenge to produce a dense and smooth Cu–Zn–Sn–S precursor from the electrolyte solution. Fig. 1a shows the typical cyclic voltammograms (CV) that was carried out in the potential window range from 0.12 to –1.3 V (vs. Ag/AgCl) to investigate the growth parameters and optimize the potential of co–electrodeposited Cu–Zn–Sn–S precursors. It also shows the reduction peak potentials for Cu(II), Sn(II) and Zn(II) at the studied concentration are –0.05 V, –0.45 and –0.83 V (vs. Ag/AgCl), respectively. The result indicates that the reduction potential gap between Zn and Cu become smaller (E_{Cu}–E_{Zn} = 0.05 V + 0.83 V = 0.88 V) in comparison with 0.14 V and –0.96 V (> 1.1 V) for Cu(II) and Zn(II) ions due to the addition of the citrate in electrolyte. In addition, the reduction potential of Cu slightly shifts toward less negative potential with increasing Cu(II) concentration, which indicates that Cu(II) concentration might affect the Cu content in the CZTS absorber layer. A further negative shift in potential results in the decrease of the cathodic current density until the potential reaches –1.2 V (vs. Ag/AgCl), where the evolution of hydrogen begins (visible bubble formation). Based on the obtained results in Fig. 1a, the co–electrodeposited potential was selected to be –1.15 V (vs. Ag/AgCl) and the current density–time behavior is shown in Fig. 1b.

Table 1. Chemical compositions and composition ratios of the sulfurized CZTS thin films co–electrodeposited from precursor solutions with different Cu(II) concentrations.

Sample ID	Elemental component (at %)				Composition ratio		
	Cu	Zn	Sn	S	Cu/(Zn+Sn)	Zn/Sn	S/Metal
CZTS(05)	20.55	16.44	12.42	50.59	0.71	1.32	1.02
CZTS(10)	21.97	15.63	11.76	50.64	0.80	1.33	1.03
CZTS(15)	22.71	15.26	11.32	50.71	0.85	1.35	1.03
CZTS(20)	24.33	14.69	10.75	50.23	0.96	1.37	1.01

The composition of the sulfurized CZTS thin films is very likely related to their electrical properties. For high–efficiency CZTS solar cells, there is an empirical rule that the Cu/(Zn +Sn) and Zn/Sn ratios of 0.75–1 and 1–1.25, respectively.[19] To investigate the effects of Cu content on the quality of CZTS thin films, the different Cu(II) concentrations (5.0, 10, 15 and 20 mM) were utilized in the precursor solutions. Table 1 and Figure S1 show the elemental compositions of the CZTS thin films from energy dispersive X–ray spectroscopy (EDS). The content of Cu increases almost linearly while that of Zn and Sn decreases in all CZTS thin films, which reveals that the amount of Cu in these thin films gradually increase with the increase in Cu(II) concentration. The average compositions of all films are the Cu/(Zn+Sn) ratio of <0.96, Zn/Sn ratio of >1.32 and S/Metal >1.0 (sulfur in ~50% excess), which suggests that the highly desired Cu–poor and Zn–rich CZTS absorber layers can be formed. These composition ratios for the cations diverge a bit from other best compositions reported literatures,[13,19,21] where the ratio of Cu/(Zn+Sn)=0.8 and Zn/Sn=1.2 are generally reported to yield the best results. All CZTS thin films have different compositions even though the same sulfurization process was applied to all precursors with different Cu(II) concentrations. Thus, it is necessary to control a

Cu–poor state in CZTS, the Cu content in finally produced CZTS thin films can be easily adjusted by changing the concentration of Cu(II) in the precursor solution, without any additional procedures.

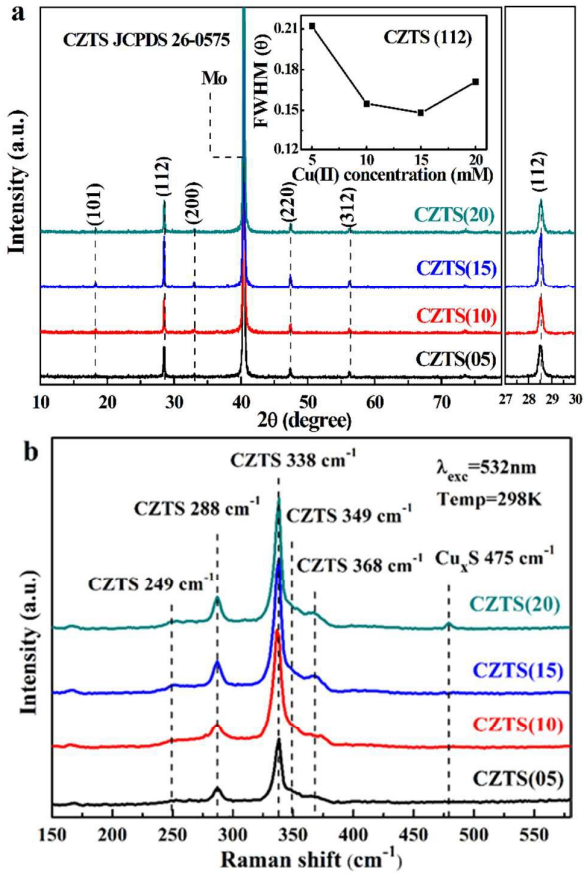

Fig. 2(a) XRD patterns and (b) Raman spectra of the sulfurized CZTS thin films co–electroplated with various Cu(II) concentrations.

The XRD patterns of the as–synthesized CZTS thin films with different Cu(II) concentrations (5, 10, 15 and 20 mM) co–electroplated onto Mo glass/substrates are shown in Fig. 2a. The main diffraction peaks of the sulfurized CZTS thin films at the 2θ values of 18.21°, 28.53°, 32.98°, 47.33° and 56.18°, apart from the peaks arising from the Mo underlayer, can be attributed to the (101), (112), (200), (220) and (312) planes of kesterite CZTS structure (JCPDS 26–0575) with a strong preferential orientation in (112) direction, indicating the formation of the CZTS phase.[28] The enlarged (112) peak region in the 2θ of 27.0–30.0° gradually increases and the full–width at half–maximum (FWHM) decreases with the Cu(II) concentration increase from 5 to 15 mM, but the (112) peak drops and the FWHM increases with further increasing the Cu(II) concentration to 20 mM. These changes demonstrate the enhancement in the crystallinity of CZTS thin films, which can presumably be attributed to the increase in the predicted grain size, as observed in the surface and cross–sectional SEM images of CZTS thin films in Fig. 3a–c and 3e–g.

Although XRD techniques are commonly used to determine the crystalline structure of phases, they cannot be distinguished clearly here because the (112) peak of the kesterite CZTS ($2\theta_{CZTS}$=28.53°, JCPDS 26–0575) is very close to (111) peak of cubic ZnS ($2\theta_{ZnS}$=28.50°, JCPDS 36–1450) and if co-existed in the synthesized films. Therefore, Raman scattering spectroscopy with 532 nm excitation wavelength (red spectra) was used to confirm the presence of kesterite CZTS and/or secondary phases. Raman peaks corresponding to the kesterite CZTS phase are observed at 249, 288, 338, 349 and 368 cm^{-1} in Fig. 2b, agreeing well with the reported characteristic CZTS vibration modes.[23,24,26,28] Raman spectra also reveals the presence of an additional peak at 475 cm^{-1} assigned to Cu_xS for only CZTS(20) thin film with excess Cu,[24,31] which could lead to the decrease in the electrical performance due to the low energy gap and high interfacial recombination velocity. Besides, it can be observed that the intensity of peak at around 338 cm^{-1} firstly decreases and then increases with increasing the Cu(II) concentration, the same trend is consistent with the XRD results (Fig. 2a).

The ZnS is a well-known secondary phase present in CZTS absorber layers,[19,22] but it is also difficult to precisely identify the ZnS phase using Raman spectra with a 532 nm excitation wavelength. For further phase elucidation, Raman analysis was performed with a 325 nm excitation wavelength (blue spectra) similar to the ZnS band gap (~3.7 eV). The Raman spectrum of the same samples is significantly different, as shown in Figure S3, where the peak at 345 cm^{-1} can be assigned to the primary vibration mode of ZnS,[22] yet the CZTS Raman characteristic peaks are very weak. The high intensity of this peak is because of the existence of a quasi–resonant excitation of the ZnS vibrational mode at this excitation condition, in which Raman spectroscopy becomes extremely sensitive in the detection of even small quantities of ZnS in the sample.[33] The intensity of ZnS peak becomes relatively weak and very broad with increasing Cu(II) concentration, which indicates the content of ZnS in CZTS films decrease in combination with the compositions in Table 1. The experimental results indicate that the secondary phase of ZnS co-exists mainly at the surface of the CZTS thin film, rather than in the region close to the CZTS/Mo interface.[22] More importantly, the selective removal of the superficial ZnS secondary phases could be removed more easily by etching in deionized water, cyanide and hydrochloric acid, which becomes an effective method to improve solar cell performance. Here our CZTS thin films were handled by RF sputtering for 10 min. This process is important to realize a clean interface at the p–n junction.

X–ray photoelectron spectroscopy (XPS) was carried out to investigate the oxidation states of the CZTS thin films' surface elements (Figure S4). Two characteristic Cu 2p core level spectra clearly shows binding energy values for the Cu 2p1/2 and Cu 2p3/2 peaks at 952.4 and 932.6 eV with a peak splitting of 19.8 eV, indicative of Cu(I). The Zn 2p1/2 and 2p3/2 peaks located at 1045 and 1022 eV show a peak separation of 23 eV, revealing the formation of Zn(II) state. In the Sn 3d core level, 3d3/2 and 3d5/2 peaks are located at 494.5 and 486.1 eV, respectively, corresponding to the Sn(IV) state with a characteristic binding energy of 8.4 eV. Finally, the S 2p1/2 and 2p3/2 peaks in the spectra are located at 162.5 and 161.3 eV with a peak splitting of 1.18 eV, consistent with S in sulfide compounds. It is clear that the XPS analysis confirms that in these films, the elements are in the valence states of Cu(I), Zn(II), Sn(IV) and S(II), respectively.

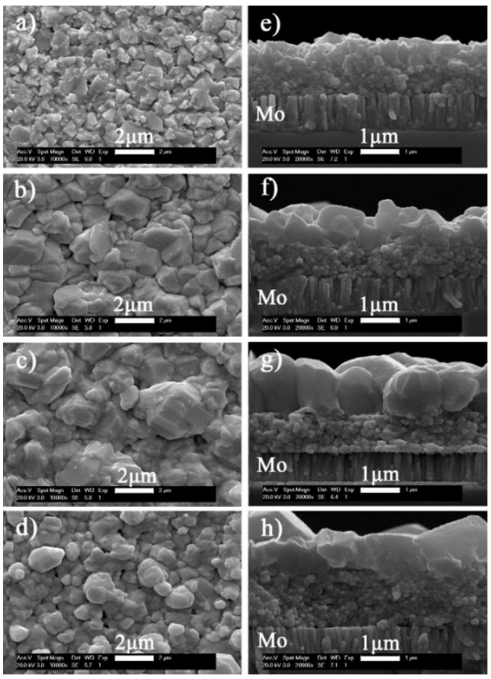

Fig. 3 Surface and cross sectional SEM images of the sulfurized CZTS thin films obtained from: (a, e) CZTS(05), (b, f) CZTS(10), (c, g) CZTS(15) and (d, h) CZTS(20).

Fig. 3 shows surface and cross–sectional SEM images of CZTS thin films deposited from different Cu(II) concentrations. Clearly, there are significant differences in average grain sizes ranging from 0.9 μm for CZTS(05), 1.8 μm for CZTS(10), 2.0 μm for CZTS(15) to 1.1 μm for CZTS(20). Moreover, the MoS_2 layer is not observed between the CZTS absorber layer and the Mo back contact. When the Cu(II) concentration increases from 5 to 15 mM, the grain size of CZTS thin film becomes larger, the film surface is denser, and isolated grains with large size and well–defined boundaries are formed, as evident in Fig. 3a–c. Furthermore, the improvement of crystallinity of CZTS thin films is also consistent with the above results of XRD and Raman. This may be due to the fact that Cu_xS phase as a flux induces the liquid phase densification and crystallization, in accordance with the results also obtained in co-evaporated CZTS and CIGS thin films,[32,34] because it has a relatively low melting point. The cross–section images of the CZTS(05, 10 and 15) thin films are shown in Fig. 3e–g. It is found that the increase in Cu(II) concentration results in a thicker large–grained top layer and a reduction in the fine–grained nanocrystalline bottom layer. The similar bi–layered structure was also observed previously in this material.[26–28] The large grains with less grain boundaries are beneficial for device performance due to less opportunity for recombination of photogenerated carriers at the grain boundaries and/or increased carrier mobility.[28] But when Cu(II) concentration rises up to 20 mM, the grain size of CZTS(20) thin film begins to reduce; corresponding cross–sectional image shows the thicknesses of small–grain grains significantly increases compared with other CZTS thin films. Finally, we could draw the conclusion that the optimal Cu(II) concentration is 15 mM, since the corresponding CZTS(15) thin film has the best crystal quality considering its strongest peak of XRD and Raman.

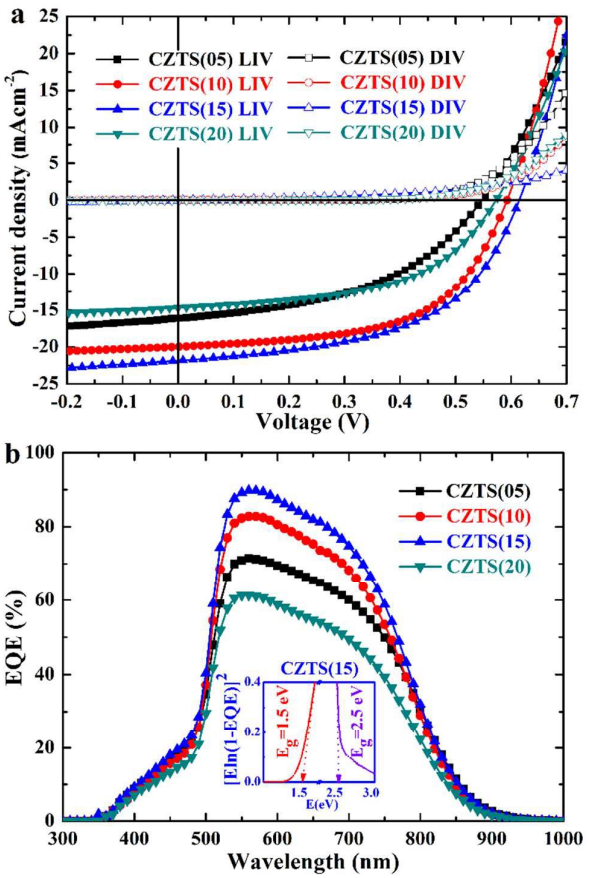

Fig. 4(a) Current density–voltage (J–V) characteristics of four CZTS solar cell devices measured in dark and under AM1.5 simulated illumination. (b) EQE measurements of the corresponding CZTS solar cells; inset: the band gap was determined by plotting $[Eln(1–EQE)]^2$ vs. E curve.

Table 2. Photovoltaic parameters of the CZTS solar cells derived from CZTS thin films co–electroplated with different Cu(II) concentrations.

Cells	PCE (%)	V_{oc} (mV)	J_{sc} (mA cm^{-2})	FF (%)	R_s (Ω cm^2)	R_{sh} (Ω cm^2)
CZTS(05)	4.0	546.7	16.1	45.8	25.3	400.5
CZTS(10)	6.7	592.4	19.9	57.6	13.1	682.8
CZTS(15)	7.1	614.3	21.8	55.5	12.6	669.3
CZTS(20)	4.4	572.6	14.6	52.2	20.5	612.3

The electrical device characteristics of several devices obtained from CZTS absorber layers deposited from different Cu(II) concentrations are presented in Fig. 4a, and all the device parameters are listed in Table 2. All device parameters dramatically improve with the increase in Cu(II) concentration from 5 to 15 mM, resulting in a dramatic increase in PCE from 4.0% to 7.1%; one of the devices obtained from CZTS(15) absorber layer has the best PCE of 7.1, which is the highest efficiency among all reports of CZTS solar cells prepared by co–electrodeposition. Also the series resistance (R_s) of CZTS(15) device is quite lower than that of others. The improved device performance mainly stems from enhanced the open-circuit voltages (V_{oc}), short-circuit current density (J_{sc}) and fill factor (FF). These changes are mainly attributed to the observation of a high–quality microstructure with large grains (>1 μm), free of conducting

Cu_xS and less high-resistivity ZnS, as seen in SEM and Raman analysis (see Fig. 2b, Fig. 3 and Figure S3). In comparison with the record CZTS solar cell (PCE=8.4%, FF=65.8%, V_{oc}=661 mV, J_{sc}=19.5 mA cm^{-2} and R_s=4.5 Ω cm^2),[21] the PCE in our device is predominantly limited by low FF (55.5%) due to high R_s (12.6 Ω cm^2) and low R_{sh} (669.3 Ω cm^2). This can be ascribed to the bottom of the small-grained CZTS absorber layer. Hence, it would be an optimum sulfurization conditions (temperature, pressure and time) to achieve homogeneous CZTS absorber layers with large densely packed grains. The additional increase in a MgF_2 antireflection coating may improve the PCE to over 7.5%. When the Cu(II) concentration is increased from 5 to 15 mM, V_{oc} significantly improves from 546.7 to 614.3 mV, which can be associated with enhanced carrier activation in the absorbers;[35] moreover, R_{sh} value of CZTS(15) device is relatively higher than that of other CZTS solar cells, as seen in Table 2. Consequently a higher R_{sh} can also give rise to a higher V_{oc}. However, the PCE of the CZTS(20) device is limited by a high R_s (20.5 Ω cm^2) and a lower V_{oc} (572.6 mV), resulting in a substantial loss in FF (52.2%). We speculate that these values could be attributed predominantly to conducting Cu_xS phase in CZTS absorber layer with small grains (see Fig. 2b and Fig. 3d, 3h) since it acts as shunting paths or block current flow[36] thereby diminishing the device performance. Further optimization of the precursor composition (Zn(II) and Sn(II) ions) is important for fabricating a CZTS absorber layer composed of a large grain size and phase purity in order to improve the device performance.

Fig. 4b shows the external quantum efficiency (EQE) of the corresponding CZTS solar cells in wavelengths ranging from 300 to 1000 nm. The wavelengths below ~520 nm (blue light collection) are slightly poorer than those reported by others,[6-15,22-27] which is consistent with a higher absorption characteristic and a lower transmittance of the sputtered CdS thin film due to slightly thicker thicknesses (150 nm) shown in Figure S5 and Figure S6, respectively. Compared to the reported electrodeposited CZTS solar cell (PCE=7.3%, J_{sc}=22 mA cm^{-2}),[26] short wavelength loss occurs at the front of the CZTS(15) solar cell (PCE=7.1%, J_{sc}=21.8 mA cm^{-2}), this effect is compensated by enhanced medium wavelength (520–750 nm) response, as shown in Figure S5. This can be explained by the fact that the sputtered CdS film has relatively good quality in Figure S7 and the inset of Figure S2. Moreover, CdS thin films deposited on both glass substrate and CZTS/Mo/glass substrate exhibit the polycrystalline diffraction peaks corresponding to hexagonal H(002)/C(111) and H(004)/C(222) planes. As the increase in Cu(II) concentration from 5 to 15 mM, the maximum EQEs of CZTS solar cells increase from ~62% to ~90% (at 560 nm), which could occur if interface recombination at medium wavelength (520–800 nm) has been improved. This improvement is consistent with a higher J_{sc} shown in Table 2, which can be explained by the fact that the absorber layer from a high Cu(II) concentration has better CZTS quality: larger grains with less grain boundaries and free of detrimental Cu_xS secondary phase. However, the EQEs in the visible range gradually decays for longer wavelength region beyond the band edge (>800 nm). This decay is most likely caused by poor minority carrier diffusion length and/or insufficient penetration of the depletion width into the absorber.[11,27] In addition, the band gaps of the CZTS(15) and CdS thin films are estimated about 1.5 eV and 2.5 eV, respectively, from the EQE spectra by fitting a plot of $[Eln(1–EQE)]^2$ vs. E near the band edge, as shown in the inset of Fig. 4b, which is in reasonable agreement with the reported values.[24,28]

4. Conclusions

In summary, we have introduced an innovative sputtered CdS buffer layer for CZTS solar cells that shows similar functionality level as a CBD–CdS buffer layer, and offers exceptional opportunities for the scalable and safe manufacture of low-cost and high-performance photovoltaic technologies. The PCE of 7.1% is the highest reported so far for co–electroplated CZTS thin film solar cells. Our results clearly show a relatively high Cu(II) concentration enhances the (112) preferred orientation and crystallinity of the absorber layers, accordingly reduces the series resistance, and apparently improves the device efficiency by the simultaneous enhancement in J_{sc}, V_{oc} and FF. However, CZTS absorber layer with an excess of Cu degrades the crystal quality, forms a CuS_x secondary phase, which is detrimental to photovoltaic performance especially V_{oc}. This work not only opens up a very important and promising route to preparing high–efficiency CZTS solar cells but also provides a critical pathway to reduce the environmental impact and enhance the continuity of the solar modules.

Acknowledgements

This project was financed by the National Science Foundation of China (61106064, 61376129 and 61474045) and Knowledge Innovation Program of the Chinese Academy of Sciences (Grant No. Y2K4401DG0).

Notes and references

1 T.K. Todorov, K.B. Reuter and D.B. Mitzi, Adv. Mater., 2010, 22, E156–E159.
2 K. Kim, I. Kim, Y. Oh, D. Lee, K. Woo, S. Jeong and J. Moon, Green Chem., 2014, 16, 4323–4332.
3 W. Shockley and H.J. Queisser, Adv. Energy Mater., 2011, 1, 732–735.
4 M.A. Green, K. Emery, Y. Hishikawa and W. Warta, Prog. Photovolt: Res. Appl., 2011, 19, 84–92.
5 M.A. Green, K. Emery, Y. Hishikawa, W. Warta and E.D. Dunlop, Prog. Photovolt: Res. Appl., 2015, 23, 1–9.
6 Y.S. Lee, T. Gershon, O. Gunawan, T.K. Todorov, T. Gokmen, Y. Virgus and S. Guha, Adv. Energy Mater. 2014, 5 1401372.
7 W. Wang, M.T. Winkler, O. Gunawan, T. Gokmen, T.K. Todorov, Y. Zhu and D.B. Mitzi, Adv. Energy Mater., 2014, 4, 1301465.
8 Y. Cao, M.S. Denny, J.V. Caspar, W.E. Farneth, Q. Guo, A.S. Ionkin, L.K. Johnson, M.Lu, I. Malajovich, D.Radu, H.D. Rosenfeld, K.R. Choudhury and W. Wu, J. Am. Chem. Soc., 2012, 134, 15644−15647.
9 W. Yang, H.S. Duan, B. Bob, H. Zhou, B. Lei, C.H. Chung, S.H. Li, W.W. Hou and Y. Yang, Adv. Mater., 2012, 24, 6323–6329.
10 T.K. Todorov, O. Gunawan, T. Gokmen and D.B. Mitzi, Prog. Photovoltaics: Res. Appl., 2013, 21, 82–87.
11 T.K. Todorov, J. Tang, S. Bag, O. Gunawan, T. Gokmen, Y. Zhu and D.B. Mitzi, Adv. Energy Mater., 2013, 3, 34–38.
12 W. Wang, M.T. Winkler, O. Gunawan, T. Gokmen, T.K. Todorov, Y. Zhu and D.B. Mitzi, Adv. Energy Mater., 2014, 4, 1301465.

13 Q. Guo, G.M. Ford, W.C. Yang, B.C. Walker, E.A. Stach, H.W. Hillhouse and R. Agrawal, J. Am. Chem. Soc., 2010, 132, 17384–17386.
14 S. Bag, O. Gunawan, T. Gokmen, Y. Zhu, T.K. Todorov and D.B. Mitzi, Energy Environ. Sci., 2012, 5, 7060.
15 H.S. Duan, W. Yang, B. Bob, C.J. Hsu, B. Lei and Y. Yang, Adv. Funct. Mater., 2013, 23, 1466–1471.
16 S. Chen, A. Walsh, J.H. Yang, X. G. Gong, L. Sun, P.X. Yang, J.H. Chu and S.H. Wei, Phys. Rev. B, 2011, 83, 125201.
17 F. Liu, F. Zeng, N. Song, L. Jiang, Z. Han, Z. Su, C. Yan, X. Wen, X. Hao and Y. Liu, ACS Appl. Mater. Interfaces., 2015, 7, 14376−14383.
18 Z. Su, J.M. R. Tan, X. Li, X. Zeng, S.K. Batabyal and L.H. Wong, Adv. Energy Mater., 2015, 1500682.
19 S. Chen, A. Walsh, X.G. Gong and S.H. Wei, Adv. Mater., 2013, 25, 1522–1539.
20 H. Katagiri, K. Jimbo, W.S. Maw, K. Oishi, M. Yamazaki, H. Araki and A. Takeuchi, Thin Solid Films, 2009, 517, 2455–2460.
21 B. Shin, O. Gunawan, Y. Zhu, N.A. Bojarczuk, S.J. Chey and S. Guha, Prog. Photovolt: Res. Appl., 2013, 21, 72–76.
22 Z. Su, K. Sun, Z. Han, H. Cui, F. Liu, Y. Lai, Y. Lai, J. Li, X. Hao, Y. Liu and M. A. Green, J. Mater. Chem. A, 2014, 2, 500–509.
23 F. Liu, K. Sun, W. Li, C. Yan, H. Cui, L. Jiang, X. Hao and M.A. Green, Appl. Phys. Lett., 2014, 104, 051105.
24 K. Woo, Y. Kim and J. Moon, Energy Environ. Sci., 2012, 5, 5340–5345.
25 K. Tanaka, Y. Fukui, N. Moritake and H. Uchiki, Sol. Energy Mater. Sol. Cells, 2011, 95, 838–842.
26 S. Ahmed, K.B. Reuter, O. Gunawan, L. Guo, L.T. Romankiw and H. Deligianni, Adv. Energy Mater., 2012, 2, 253–259.
27 F. Jiang, S. Ikeda, T. Harada and M. Matsumura, Adv. Energy Mater., 2014, 4, 1301381.
28 J. Tao, K. Zhang, C. Zhang, L. Chen, H. Cao, J. Liu, J. Jiang, L. Sun, P. Yang and J. Chu, Chem. Commun., 2015, 51, 10337–10340.
29 H. Chen, Q. Ye, X. He, J. Ding, Y. Zhang, J. Han, J. Liu, C. Liao, J. Mei and W. Lau, Green Chem., 2014,16,3841–3845.
30 A. Ennaoui, M. Lux–Steiner, A. Weber, D. Abou–Ras, I. Kötschau, H.–W. Schock, R. Schurr, A. Hölzing, S. Jost, R. Hock, T.Voß, J. Schulze and A. Kirbs, Thin Solid Films, 2009, 517, 2511–2514.
31 J. Tao, J. Liu, J. He, K. Zhang, J. Jiang, L. Sun, P. Yang and J. Chu, RSC Adv., 2014, 4, 23977–23984.
32 T. Tanaka, A. Yoshida, D. Saiki, K. Saito, Q. Guo, M. Nishio and T. Yamaguchi, Thin Solid Films, 2010, 518, S29–S33.
33 X. Fontané, L. Calvo–Barrio, V. Izquierdo–Roca, E. Saucedo, A. Pérez–Rodriguez, J.R. Morante, D.M. Berg, P.J. Dale and S. Siebentritt, Appl. Phys. Lett., 2011, 98, 181905.
34 A.M. Gabor, J.R. Tuttle, S.S. Albin, M.A. Contrears and R. Noufi, Appl. Phys. Lett., 1994, 65, 198–200.
35 J.M. R. Tan, Y.H. Lee, S. Pedireddy, T. Baikie, X.Y. Ling and L.H. Wong, J. Am. Chem. Soc., 2014, 136, 6684–6692.
36 J. Kim, H. Hiroi, T.K. Todorov, O. Gunawan, M. Kuwahara, T. Gokmen, D. Nair, M. Hopstaken, B. Shin, Y.S. Lee, W. Wang, H. Sugimoto and D.B. Mitzi, Adv. Mater., 2014, 26, 7427–7431.